Enzymatic Birch Reduction via Hydrogen Atom Transfer at an Aqua-Tungsten- bis-Metallopterin Cofactor

Seelmann, Carola S.; Huwiler, Simona G.; Culka, Martin; Strampraad, Marc J.F.; Biskup, Till; Weber, Stefan; Ullmann, G. Matthias; Hagedoorn, Peter Leon; Pierik, Antonio J.; More Authors

DOI
10.1021/acscatal.3c01781

Publication date
2023

Document Version
Final published version

Published in
ACS Catalysis

ACS Catalysis

pubs.acs.org/acscatalysis Research Article

Enzymatic Birch Reduction via Hydrogen Atom Transfer at an Aqua-Tungsten-*bis*-Metallopterin Cofactor

Carola S. Seelmann, Simona G. Huwiler, Martin Culka, Marc J. F. Strampraad, Till Biskup, Stefan Weber, G. Matthias Ullmann, Volker Schünemann, Peter-Leon Hagedoorn, Antonio J. Pierik, and Matthias Boll*

Cite This: *ACS Catal.* 2023, 13, 8631−8641 Read Online

ACCESS | Metrics & More | Article Recommendations | Supporting Information

ABSTRACT: The Birch reduction is a widely used synthetic tool to reduce arenes to 1,4-cyclohexadienes. Its harsh cryogenic reaction conditions and the dependence on alkali metals have motivated researchers to explore alternative approaches. In anaerobic aromatic compound degrading microbes, class II benzoyl-coenzyme A (CoA) reductases (BCRs) reduce benzoyl-CoA to the conjugated cyclohexa-1,5-diene-1-carboxyl-CoA (1,5-dienoyl-CoA) at a tungsten-*bis*-metallopterin (MPT) cofactor. Though previous structure-based computational studies were in favor of a Birch-like reduction via W(V)/radical intermediates, any experimental evidence for such a mechanism was lacking. Here, we combined freeze-quench and equilibrium electron paramagnetic resonance (EPR) spectroscopic analyses in H_2O, D_2O, and $H_2{}^{17}O$ with redox titrations using wild-type and molecular variants of the catalytic BamB subunit of class II BCR from the anaerobic bacterium *Geobacter metallireducens*. We provide spectroscopic evidence for a kinetically competent radical/W(V)−OH intermediate obtained after hydrogen atom transfer from the W-aqua-ligand to the aromatic ring and for an invariant histidine as a proton donor assisting the second electron transfer. Quantum mechanical/molecular mechanical calculations suggest that the unique tetrahydro state of both pyranopterins is essential for the reversibility of enzymatic Birch reduction. This work elucidates nature's solution for the chemically demanding Birch reduction and demonstrates how the reactivity of MPT cofactors can be expanded to highly challenging radical chemistry at the negative limit of the biological redox window.

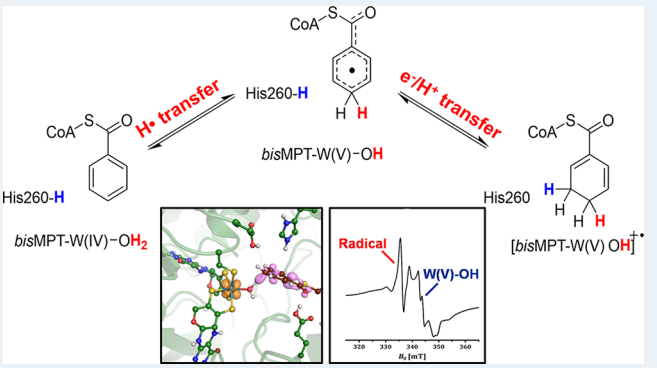

KEYWORDS: *Birch reduction, radical enzyme, tungsten, EPR spectroscopy, oxidoreductase*

INTRODUCTION

The Birch reduction, discovered almost 80 years ago, is a widely used synthetic procedure to achieve dihydro-additions to arenes usually yielding 1,4-cyclodienes.[1,2] It proceeds via single electron and proton transfer steps with the first electron transfer generating a radical anion intermediate as the rate-limiting step. This demanding reduction requires cryogenic temperatures and solvated electrons that are usually generated by dissolving alkali metals in liquid ammonia. Though this harsh procedure is still the most common method applied for the reduction of arenes to cyclic dienes, many efforts to develop ammonia-free chemical procedures have been made in recent years.[3−7] Recently, electrochemical and photochemical methodologies have been developed that may serve as alternatives to the classical Birch reduction in the future.[8−11]

Considering the non-physiological conditions of the classical Birch reduction, it is astonishing that anaerobic bacteria employ enzymes that catalyze the two-electron reduction of a homocyclic aromatic ring to a cyclic diene. These so-called benzoyl-coenzyme A (CoA) reductases (BCRs) play a key role in the globally important anaerobic degradation of aromatic compounds including lignin-derived monomers or the environmentally relevant and carcinogenic BTEX (benzene, toluene, ethylbenzene, xylene).[12,13] BCRs reduce benzoyl-CoA, the central intermediate of anaerobic degradation pathways, to cyclohexa-1,5-diene-1-carboxyl-CoA (1,5-dienoyl-CoA) at a standard redox potential of $E^{\circ\prime}$ = −622 mV (vs the standard hydrogen electrode, SHE, pH 7).[14] This redox potential is among the most negative ones in biology, and even with the most potent reductant in biology, reduced ferredoxin (Fd_{red}), this reaction is highly endergonic. The CoA ester moiety of the substrate was proposed to stabilize radical intermediates as ketyls during the Birch-like reduction of the aromatic ring (Figure 1a).[15] It is noteworthy that unlike the chemical Birch reduction, the enzymatic reaction affords the thermodynami-

Received: April 20, 2023
Revised: May 26, 2023
Published: June 15, 2023

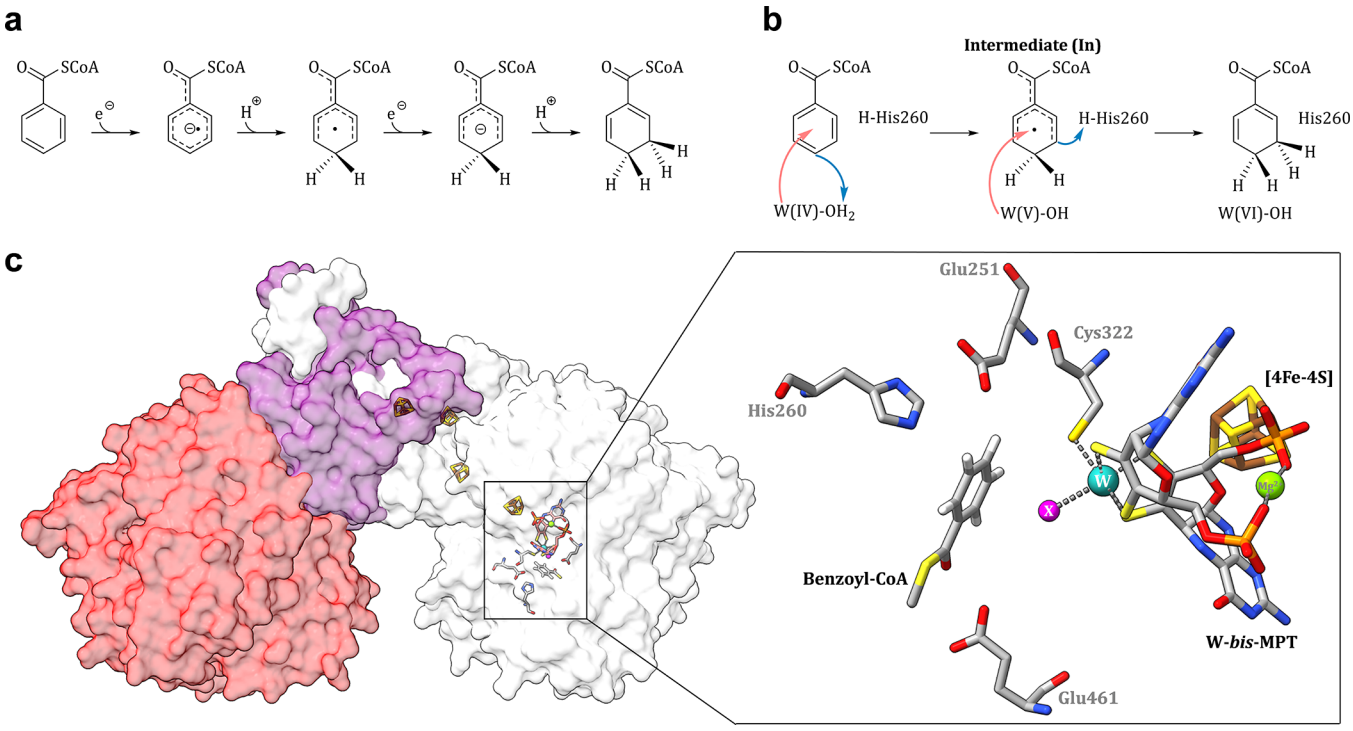

Figure 1. Enzymatic Birch reduction and the Bam$(BC)_2$ subcomplex of class II BCR from *G. metallireducens*. (a) Classical Birch reduction via single electron transfer and protonation steps adopted to enzymatic reduction of benzoyl-CoA. Note that the carbonyl of the thioester contributes to the stabilization of radical intermediates. (b) Suggested simplified mechanism of enzymatic Birch-like reduction of benzoyl-CoA at the W-*bis*-MPT in the Bam$(BC)_2$ complex based on continuum electrostatic and QM/MM calculations. (c) Left panel: X-ray structure of the Bam$(BC)_2$ heterodimer. Two BamB subunits (left one in red) are associated via two interlaced BamCs (left one in violet). Right panel: catalytic site of BamB. The substrate benzoyl-CoA (CoA-ester moiety is truncated for clarity) is flanked by the possible proton donor His260 and the sixth tungsten (W) ligand (X). Other relevant amino acid residues are explained in more detail in the text.

cally favored conjugated diene product. There are two non-related BCR classes that use fundamentally different solutions for reductive benzoyl-CoA dearomatization. The tetrameric class I BCRs contain three [4Fe−4S] clusters and drive benzoyl-CoA reduction with Fd_{red} as reductant by coupling it to a stoichiometric ATP hydrolysis (two ATP are hydrolyzed to two ADP per two electrons transferred).[16,17] The one-megadalton class II BCRs are composed of eight subunits with a Bam$[(BC)_2DEFGHI]_2$ architecture.[18] Here, reduction of benzoyl-CoA to 1,5-dienoyl-CoA is supposed to be driven by flavin-based electron bifurcation.[19] In such a process, the endergonic reduction of benzoyl-CoA by Fd_{red} is coupled to the reduction of a so far unknown high-potential acceptor by Fd_{red}.[20]

The active site subunit BamB of class II BCRs belongs to the aldehyde/ferredoxin-oxidoreductases (AOR) family of tungsten or molybdenum metallopterin (MPT) cofactor containing enzymes.[21] It has originally been purified in complex with the electron-transferring FeS cluster containing BamC subunit from the Fe(III)-respiring *δ*-proteobacterium *Geobacter metallireducens* (*G. metallireducens*).[22] The X-ray structure of Bam$(BC)_2$ crystals revealed an active site W-*bis*-MPT cofactor in which the central tungsten atom is coordinated by four dithiolene sulfurs from the two MPT moieties, by a thiolate from the conserved Cys322, and by a sixth inorganic ligand[23] (Figure 1c). The identity of the latter could not be resolved unambiguously on the basis of the crystal structure and is referred to as X-ligand here. Extended X-ray absorption fine structure spectroscopy excluded the presence of a sixth sulfur ligand and was in favor of an O-, N-, or a diatomic inorganic ligand.[23]

The fully occupied coordination sphere of the tungsten atom excludes a direct binding of benzoyl-CoA to the tungsten. Indeed, X-ray structural data of Bam$(BC)_2$ in complex with its substrate or product suggested an outer-shell electron transfer from a reduced W(IV) species via the X-ligand to the C4 of benzoyl-CoA.[23] Conserved His260 and Glu251 were proposed as possible proton donors for the Birch-like reduction mechanism. The spatial separation of the electron donor (W[IV]-X-ligand) and the proton donating amino acid functionalities was in line with the proposed Birch-like mechanism via single electron transfer and protonation steps (Figure 1a). Radical intermediates may be stabilized by the thioester carbonyl oxygen that interacts as a donor with the protonated Glu461-OE1. Such a partial protonation of the carbonyl oxygen appears to be characteristic for both BCRs.[14,24]

Based on the X-ray structural data obtained, continuum electrostatic and combined quantum mechanical/molecular mechanical methods (QM/MM) were carried out in which a number of inorganic atoms were probed as potential sixth X-ligand.[25] These calculations favored an aqua ligand as the sixth ligand of the W(IV)-atom and suggested a variant of the previously proposed Birch-like mechanism (Figure 1b). In this variant, catalysis would be initiated by hydrogen atom transfer from a W(IV)−OH_2 species to the substrate yielding W(V)−OH and a neutral substrate radical. The second electron transfer from the metal cofactor to the substrate could then be assisted by protonation by His260. Calculations suggested that

https://doi.org/10.1021/acscatal.3c01781
ACS Catal. 2023, 13, 8631−8641

the two MPT moieties may participate in the second electron transfer, and the cationic pterin radical formed could retain the W(V) state. Reduction of the oxidized cofactor by two electrons and product/substrate exchange closes the cycle.

The QM/MM calculations were in favor of a Birch-like reaction mechanism in which the strict coupling of electron transfer and protonation steps facilitates enzymatic reduction. However, any experimental evidence for the nature of the sixth W-ligand and, consequently, for the proposed hydrogen atom transfer mechanism is lacking. In order to provide the first experimental evidence for the mechanism of an enzymatic Birch reduction, we carried out an in-depth EPR analysis of the Bam(BC)$_2$ complex under pre-steady state and equilibrium conditions using wild-type and molecular variants in differently labeled solvents. Together with redox titrations and extended QM/MM calculations, we provide experimental evidence for the nature of the sixth W-ligand and for catalytically competent reaction intermediates, which provide a solid basis for a hydrogen atom transfer-based Birch-like mechanism.

EXPERIMENTAL SECTION

Coenzyme A and Its Thioesters. CoA was obtained from BioFroxx. CoA esters were synthesized from benzoic acid ($^{12}C_6$ or [Ring]-$^{13}C_6$) or 1-cyclohexene-1-carboxylic acid as described earlier.[26] Cyclohexa-1,5-dienoyl-CoA was enzymatically synthesized from benzoyl-CoA with enriched class I BCR and the products were purified by preparative high-performance liquid chromatography (HPLC).[27]

Homologous Gene Expression, Enzyme Production, and Formation of Molecular Mutants. Originating from plasmid pGM2087e1,[18] two variants were generated in which the active site His260 was exchanged for an asparagine or an alanine by using the Q5 Site-Directed Mutagenesis Kit (New England Biolabs, Inc., (NEB), Ipswich, MA, USA). The resulting plasmids were termed pGM2087e6 (H260N) and pGM2087e7 (H260A) (Table S2). All polymerase chain reaction (PCR) amplifications were performed with Q5 High-Fidelity Polymerase (NEB, Ipswich, MA, USA). Ligation mixtures were transformed into *E. coli* NEB 5-alpha by heat shock transformations and plated onto agar plates containing 50 μg mL^{-1} kanamycin sulfate. Plasmids were isolated from *E. coli* with the QIAprep Spin Miniprep Kit (Quiagen, Hilden, Germany) according to the manufacturer's instructions. Orientation of the insert and its sequence as well as the adjoining vector regions were sequenced by Sanger sequencing at GATC or Eurofins. *G. metallireducens* was transformed via electroporation as described previously.[28] The presence of the plasmid was confirmed by PCR using appropriate primers and RedTaq Mastermix (Genaxxon Bioscience, Ulm, Germany).

Genetically modified *G. metallireducens* GS-15 strains were cultivated at 28 °C under strictly anoxic conditions in the presence of 50 μg mL^{-1} kanamycin sulfate in a mineral salt medium[29] with either benzoate or cyclohexane carboxylic acid (CHC)[30] as carbon source and nitrate as electron acceptor up to the 200 L scale. ^{15}N-labeled BamBC was produced from *G. metallireducens* GS-15 pGM2087e1 under strictly anoxic conditions in the 2 L scale in mineral salt medium containing $Na^{15}NO_3$ (Sigma-Aldrich), $^{15}NH_4Cl$ (Eurisotop), and benzoate as carbon source. Cells were harvested anaerobically in the exponential growth phase by centrifugation (20,000*g*) and stored in liquid nitrogen until further use. The Strep-tagged variants of Bam(BC)$_2$ (WT, H260N, and H260A) were purified as described previously.[18]

Protein Analyses. Proteins were routinely analyzed via sodium dodecyl sulfate-polyacrylamide gel electrophoresis[31] and stained using SimplyBlue SafeStain (Invitrogen, Darmstadt, Germany). Gel pictures were acquired with a ChemiDoc XRS+ and the Image Lab 3.0 software (Bio-Rad, Hercules, USA). Protein concentrations were determined by the method established by Bradford, using bovine serum albumin for calibration.[32] To verify protein identities, the respective bands were excised, and proteins were prepared for liquid chromatography-mass spectrometry (LC−MS) analysis by tryptic in-gel digest accompanied by the reduction by dithiothreitol and alkylation of cysteine residues with iodoacetamide. LC−MS analysis was performed with an Acquity I-class UPLC System (Waters, Milford, USA) coupled to a Synapt G2-Si quadrupol-time-of-flight (Q-TOF) mass spectrometer (Waters). MS measurements were evaluated with MassLynx V4.1 (Waters), and proteins were identified with PeptideLynx Global Server (Waters).

For the identification of peptides by liquid chromatography-electrospray ionization (LC-ESI) QTOF, 10 μL samples were applied to a Peptide CSH 1.7 μm C_{18} column (150 × 2.1 mm^2, waters) at a flow rate of 0.04 mL min^{-1} with 1% acetonitrile/0.1% formic acid (v/v) in water/0.1% formic acid (v/v). After 2 min run time, the acetonitrile/0.1% formic acid concentration increased linearly to 40% within 38 min, then to 85% within 2 min. The mass spectrometer with ESI ionization was operated in the HDMS^E Resolution mode with positive polarity and a capillary voltage of 3 kV, a cone voltage of 25 V, 40 V source offset, 120 °C source temperature, 350 °C desolvation temperature, 800 L h^{-1} desolvation gas flow (N_2), 50 L h^{-1} cone gas flow (N_2) as well as 6 bar nebulizer pressure. Collision-induced dissociation of precursor ions was performed using a transfer collision energy ramp of 20−45 V and argon gas. Peptides were identified by the PeptideLynx Global Server (Waters) and mapped against the translated genome of *G. metallireducens* GS15 (taxonomic identifier 269799) downloaded from UniProt.

DCO Activity Assay. The 1,5-dienoyl-CoA/methyl viologen oxidoreductase (DCO) activity was determined as described earlier[22] with 0.2 mM 1,5 dienoyl-CoA and 0.5 mM methyl viologen at pH 6.8.

Redox Titrations. Redox titrations of Bam(BC)$_2$ were conducted under anaerobic conditions at 25 °C. Bam(BC)$_2$ was transferred into redox titration buffer (100 mM TEA, 5 mM $MgCl_2$, 5% PEG at pH 8.0) using the PD-10 desalting column (Sephadex G-25 M, GE Healthcare). For poising redox potentials, different 1,5-dienoyl-CoA/benzoyl-CoA ratios with a total concentration of 1 mM were added to ≈ 130 μM BamBC. Samples were incubated ≈1 min at room temperature before the EPR samples were frozen in liquid nitrogen under anaerobic conditions. All samples of this redox titration were measured with EPR experiments at 80 K and 5 mW. $E^{\circ\prime}$ (W[V/VI]) was calculated based on the 1,5-dienoyl-CoA/benzoyl-CoA concentration present in the EPR sample at the time point of freezing with a midpoint potential of $E^{\circ\prime}$ = −622 mV for 1,5-dienoyl-CoA/benzoyl-CoA.[14] A sigmoidal fit for the data points was performed with GraphPad Prism 6.

EPR Spectroscopy. Enzyme preparations were transferred into EPR buffer (200 mM TEA, 5 mM $MgCl_2$, 5% PEG 4000, pH 8.0) by passing over a desalting column (PD MiniTrap G-25, SephadexTM G-25 Medium, GE Healthcare, Munich, Germany) and reconcentration in ultrafiltration spin columns with a molecular weight cut-off (MWCO) of 10 or 30 kDa

https://doi.org/10.1021/acscatal.3c01781
ACS Catal. 2023, 13, 8631−8641

(Vivaspin 4, Sartorius, Göttingen, Germany) by centrifugation at ∼2900*g*. If not indicated otherwise, EPR samples had a final concentration of 200 μM Bam(BC)$_2$ and 4 mM of respective CoA ester.

X-band EPR measurements were conducted as described previously.[23] For this purpose, samples were frozen in synthetic-quartz (Ilmasil PS) X-band EPR sample tubes (3.0 mm inner diameter, 3.8 mm outer diameter, 180 mm length, of QSIL GmbH Ilmenau, Langewiesen, Germany). Samples were stored in liquid nitrogen until measurement. X-band spectra were recorded with a commercial spectrometer (Bruker EMX, Bruker, Rheinstetten, Germany) in conjunction with a high-Q resonator (Bruker 4119-HS-W1) and bridge ER041 MR (Bruker). The spectrometer was equipped with a cryo setup for cooling with liquid helium consisting of a cryostat (Oxford ESR900, Oxford Instruments, Abington, U.K.) and a temperature controller (Oxford ITC 503) adjusting temperature with an accuracy of ±0.1 K. Spectra were recorded at different temperatures ranging from 40 to 180 K with ∼9.40 GHz microwave (MW) frequency. The magnetic field was corrected with a Li/LiF standard, which exhibits one very narrow resonance line with $g_{Li/LiF}$ = 2.002293 ± 0.000002.[33] Li/LiF spectra were recorded at 40 and 80 K with ∼9.39 GHz MW frequency, 20 μW MW power, 0.05 mT modulation amplitude, 100 kHz modulation frequency, and 81.92 ms conversion time and time constant. Power sweeps were conducted from 10 mW to 20 μW by 3 dB steps at 40−180 K on a sample with ∼131 μM BamBC incubated for ∼1 min with 1 mM 1,5-dienoyl-CoA before freezing. Linearized power plots to evaluate saturation of a signal were performed by plotting the square root of the power in mW versus arbitrary units of the EPR signal.[34] Alternatively, EPR spectra were recorded with a Bruker Elexsys E580 X-band EPR spectrometer (digitally upgraded) and a Bruker pulsed MW bridge E580-1010 equipped with a 4122HQE cavity, a liquid nitrogen finger dewar or ESR 900 helium flow cryostat (Oxford Instruments) with a cryocooling system composed of a Stinger closed-cycle cryostat (Cold Edge Technologies) linked to an F-70 helium compressor (Sumitomo).

For samples in D_2O, 400 μL Bam(BC)$_2$ was diluted tenfold in redox buffer prepared in D_2O (99.8%, Carl Roth GmbH; 200 mM TEA, 5 mM $MgCl_2 \times 6H_2O$, at calculated pD 8.2).[35] This solution was incubated for at least 2 h at 6 °C and concentrated (30 kDa MWCO) to the initial concentration. This procedure was repeated four times. Bam(BC)$_2$ in D_2O buffer with 5% [w/v] PEG) was mixed with 1,5-dienoyl-CoA, and samples were frozen after 1 min of incubation at room temperature in X-band EPR tubes. CoA esters added to the D_2O exchanged samples were solved in D_2O redox buffer with 5% (w/v) PEG.

For analyzing the radical signal (Figure S4), Bam(BC)$_2$ WT or ^{15}N-Bam(BC)$_2$ in H_2O redox buffer with 5% [w/v] PEG was incubated with 1,5-dienoyl-CoA with natural abundance (n.a.) or ring-$^{13}C_6$-1,5-dienoyl-CoA for ∼1 min at room temperature prior to freezing.

$H_2{}^{17}O$-EPR buffer was prepared by lyophilization of a defined volume of H_2O-based EPR buffer. The dried powder was resolved in $H_2{}^{17}O$ under anaerobic conditions. 200 μL of 330 μM BamBC was concentrated to ∼50 μL (Amicon Ultra, 0.5 mL, 10 kDa MWCO, Merck, Darmstadt, Germany), diluted fivefold in $H_2{}^{17}O$-EPR buffer, and incubated for 2 h at 10 °C. The sample was again concentrated to ∼50 μL, diluted fivefold in $H_2{}^{17}$ O-EPR buffer, and incubated for 2 h at 10 °C. Finally, the sample was concentrated again to ∼50 μL and diluted to a final volume of 270 μL that was subsequently mixed with 30 μL of 40 mM 1,5-dienoyl-CoA in $H_2{}^{17}O$-EPR buffer, transferred into an X-band EPR tube, and frozen in liquid nitrogen under anaerobic conditions.

Simulation of EPR data was conducted with the EasySpin toolbox.[36]

Pre-Steady-State EPR. Rapid freeze-quench (RFQ) experiments were performed with a System 1000 apparatus (Update Instruments, Madison, USA) under anaerobic conditions. For this purpose, all lines were purged with anaerobic reaction buffer prior to sample loading, and the whole setup was kept under steady nitrogen flow throughout sample preparation. For one batch 500 μL of Bam(BC)$_2$ (400 μM) and 500 μL of 1,5-dienoyl-CoA (8 mM) in D_2O, reaction buffer (pD 8.0) was mixed and immediately quenched by spraying into a cold fluid isopentane bath at −110 °C. In there, an EPR tube was connected to a funnel, both completely immersed into the isopentane bath. The frozen material obtained was packed at the bottom of the EPR tube using a packing rod made of Teflon. After completion of packing, samples were immediately transferred into liquid nitrogen. In microsecond freeze hyperquenching (MHQ)[37] experiments 400 μM BamBC and 8 mM 1,5-dienoyl-CoA (200 μM and 4 mM final concentrations, respectively) were mixed 1:1 (v/v) at various flow rates. The system was continuously purged with anaerobic water and, additionally, the loops for loading enzyme and substrate were purged with anaerobic D_2O reaction buffer prior to sample loading. The mixed solutions were sprayed as a free-flowing jet under a vacuum (30 mbar) on a rotating plate (6000 rpm) previously cooled down with liquid nitrogen. After the samples were sprayed, additional liquid nitrogen was immediately poured into the rotor to keep the powder cold. The powder was scraped off the rotor plate, packed in EPR tubes, and stored at 77 K for EPR spectroscopic analysis.

Computational Analyses. The setup for the computational analyses has been described previously.[25]

RESULTS AND DISCUSSION

1,5-Dienoyl-CoA Induced EPR Signals of Bam(BC)$_2$. In a previous preliminary EPR spectroscopic analysis of wild-type Bam(BC)$_2$, the enzyme as isolated exhibited a 40 K EPR spectrum that was assigned to a W(V) species with features at g = 2.013, 1.982, and 1.895; it disappeared upon reduction by 1,5-dienoyl-CoA (15-fold excess, reverse reaction).[22] Here, we used the recently established homologous production of Strep-tagged Bam(BC)$_2$ to obtain sufficient amounts of enzyme for detailed EPR spectroscopic analyses (Figure S1).[18] Further, we increased the triethanolamine/HCl buffer concentrations from 20 to 200 mM to exclude a pH shift upon the addition of high concentrations of CoA esters that routinely contained residual formic acid from the HPLC purification buffer.

Using this setup, Strep-tagged Bam(BC)$_2$ as isolated exhibited a 77 K W(V) EPR signal with similar g-values compared to that published earlier[22] (Figure 2a); it is henceforth referred to as a resting-state signal. However, in contrast to the previous study, the addition of 1,5-dienoyl-CoA (10−20-fold excess) resulted in a novel strong EPR signal, whereas the W(V) signal of the as isolated enzyme disappeared (Figure 2b,c). This new type of signal strictly depended on reduction with 1,5-dienoyl-CoA but was never observed with artificial reductants like dithionite or Ti(III)-citrate. Its g_{av} < 2, visibility up to 180 K, and the pronounced hyperfine pattern is

https://doi.org/10.1021/acscatal.3c01781
ACS Catal. 2023, 13, 8631−8641

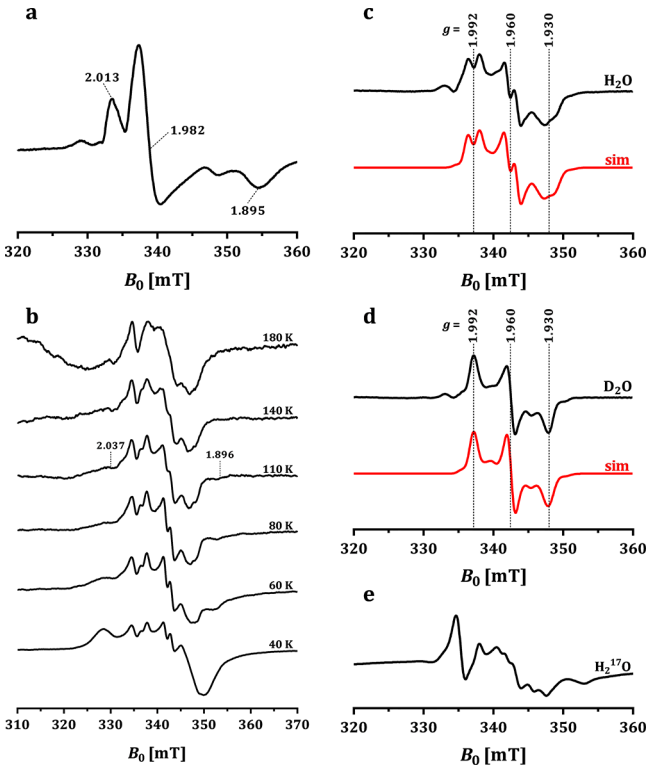

Figure 2. Steady-state EPR spectroscopy of Bam(BC)$_2$. (a) Spectrum in the as isolated state at 77 K. (b) Temperature dependency of the EPR spectrum of Bam(BC)$_2$ obtained after the addition of 5 mM 1,5-dienoyl-CoA, the *g*-values point to broad shoulders assigned to a slowly relaxing [4Fe−4S]$^{+1}$ cluster probably interacting with the W(V). Spectra were normalized to the respective total intensities. (c) 1,5-Dienoyl-CoA induced W(V) signal in H_2O buffer plus simulation (red). (d) Same as (c) but in D_2O plus simulation (red). (e) 77 K spectra in the presence of 1,5-dienoyl-CoA in $H_2{}^{17}O$. Spectra were recorded at 5 mW microwave power, 0.3 mT modulation amplitude, 100 kHz modulation frequency, and 81.92 ms conversion time. Simulation parameters of (c) were for W(V) g_W = (1.930, 1.960, 1.992) and *A* = 130, 130, 90 MHz (^{183}W, at natural abundance) interacting with a proton with A(^{1}H) = (41, 37, 45 MHz). Simulation parameters of (d) were identical, except for ^{2}H coupling constants which were 6.51 fold lower than those for ^{1}H. *g*-strain = (0.0095, 0.0060, 0.0074).[36] An isotropic radical signal simulated with *g* = 2.0028 was substracted from the spectra shown in (c) and (d).

typical for a W(V) species with well-resolved ^{1}H superhyperfine coupling and less well-resolved ^{183}W (*I* = 1/2, 14.3% natural abundance) hyperfine coupling. When the sample was prepared in D_2O, the prominent superhyperfine coupling with the single ^{1}H nucleus was lost (Figure 2d). This finding indicates that W(V) has a single solvent exchangeable proton in close proximity. The W(V) species always appeared together with an almost isotropic feature around 2.003 that is assigned to a radical species. The spin concentration ratio W(V)/radical was approximately 15:1. Similar to the W(V) signal, the isotropic signal strictly depended on reduction with the product 1,5-dienoyl-CoA, and was visible even at 180 K. The W(V)/radical signals were accompanied by broad wing-like features outside the low- (*g* = 2.037) and high-field range (*g* = 1.896) of the W(V) signal that remained visible up to 110 K (Figures 2b and S2). They are assigned to a form of the enzyme in which W(V)-*bis*-MPT and the [4Fe−4S]$^{+1}$ cluster near the W-atom (8.7 Å)[23] are spin coupled. Assuming that the pyranopterin moiety is involved in electron transfer, the edge-to-edge distance to the [4Fe−4S] cluster would even be even closer, i.e., 4.8 Å. By decreasing the temperature from 80 K to 40 K, the W(V) and radical species were only marginally saturated at 5 mW MW power, which supports the proposed magnetic interaction with the nearby [4Fe−4S]$^{+1}$ cluster of BamB.

At 40 K, novel broad features with peak intensities at 1.917 and 2.045 appeared in the 1,5-dienoyl-CoA reduced sample that are assigned to the three low-spin [4Fe−4S]$^{+1}$ clusters of the BamC subunit (Figures 2b and S2), which also are magnetically coupled due to their distances of 10−13 Å.[23] The 1,5-dienoyl-CoA induced W(V)/radical EPR signal in H_2O/D_2O, respectively, showed an increased reduction of the nearby [4Fe−4S] cluster at higher pH/pD values; at pH/pD 9, the signal mostly disappeared (Figure S3). By subtracting the spectrum obtained at pD 9 from that of pD 6, the contribution of the spin-coupled [4Fe−4S]$^{+}$ cluster could be minimized yielding a higher resolved W(V) signal including its ^{183}W (super)hyperfine coupling features (Figure S3c). Further subtraction of the simulated radical signal yielded a well-defined W(V) signal with g_{xyz}-values of 1.930, 1.960, and 1.992 and hyperfine coupling $A(^{183}W)$ of 130, 130, and 90 MHz, respectively (Figure 2d). Using these fixed values, the superhyperfine coupling constants for the single proton in H_2O were $A(^1H)$ = (41, 37, 45 MHz) (Figure 2c).

Hydroxyl as a Sixth Ligand of the Active Site W(V) Cofactor. The results obtained so far suggest that a solvent-exchangeable proton is bound in the vicinity of the tungsten. This finding rather excludes diatomic −CO or −CN as sixth ligands and favors a W(V)−SH or W(V)−OH species. To distinguish between the latter two possibilities, the $H_2{}^{16}O$ solvent was exchanged by $H_2{}^{17}O$ (>95%, 0.037% natural abundance) with ^{17}O having a nuclear spin of *I* = 5/2. The 77 K spectrum obtained in $H_2{}^{17}O$ showed a marked change of the hyperfine pattern in comparison to the one obtained in $H_2{}^{16}O$ (Figure 2e). A reliable simulation of the $H_2{}^{17}O$ spectrum was intrinsically hampered by the presence of multiple interacting nuclei (^{183}W, ^{1}H, and ^{17}O) with the already complex EPR signals of interacting W(V), radical, and [4Fe−4S]$^{+}$ cluster. Taken together, the loss of hyperfine interaction in D_2O vs H_2O and the gain of additional hyperfine interactions in $H_2{}^{17}O$ vs $H_2{}^{16}O$ leaves little doubt of the presence of a W(V)−OH species in Bam(BC)$_2$ during 1,5-dienoyl-CoA aromatization. These findings are in perfect agreement with previous continuum electrostatics and QM/MM calculation-based suggestions, and strongly support a hydrogen atom transfer from a W(IV)−OH_2 species to the aromatic ring yielding the W(V)−OH species and a radical during catalysis.[25]

To further investigate the W(V)−OH derived EPR signal, spectra of samples with pH-/pD-values between pH 6 and 9 were recorded. In this range, no significant change of the W(V) signal was observed, though at pH 9 it showed less than 20% intensity (Figure S3). This result indicates a pK_a value of the W(V)−OH species out of the tested pH range. The decrease of the W(V)−OH EPR signal at pH 9 can be explained by a reduction of the W(V)−OH to the diamagnetic W(IV)−OH_2 or [W(IV)−OH]$^-$ species as a result of the pH dependence of the redox potential of the benzoyl-CoA + 2 H^+/1,5-dienoyl-CoA redox couple. Assuming a decrease of 60 mV per increasing pH unit, the redox potential would shift from $E^{\circ\prime} \approx$ −620 mV (pH 7) to $E^{\circ\prime} \approx$ −740 mV (pH 9).[14]

Redox Titrations Indicate an Exceptional Low Redox-Potential of the Tungsten Cofactor. The benzoyl-CoA + 2

https://doi.org/10.1021/acscatal.3c01781
ACS Catal. 2023, 13, 8631−8641

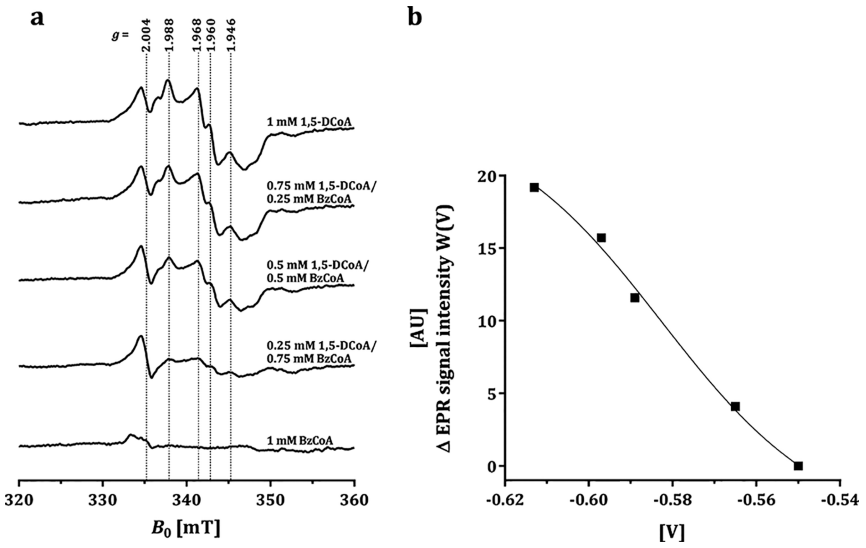

Figure 3. Redox titration of the W(V) signal of Bam(BC)$_2$ in the presence of different ratios of benzoyl-CoA/1,5-dienoyl-CoA (BzCoA/1,5-DCoA). (a) EPR spectra measured at 77 K with 5 mW power, 0.3 mT modulation amplitude, 100 kHz modulation frequency, and 81.92 ms conversion time. All spectra were normalized to the same number of scans. (b) Fit of the W(V) amplitude between g = 1.968 and 1.953 to a Nernst curve with a midpoint of −583 mV for the W(VI/V) transition with R^2 = 0.997. The redox potential W(VI/V) transition is estimated from the initial benzoyl-CoA/1,5-dienoyl-CoA ratios with $E^{\circ\prime}$ = −622 mV.[14]

H^+/1,5-dienoyl-CoA redox potential of $E^{\circ\prime}$ = −622 mV vs SHE suggests very low redox potentials of the W(VI/V/IV) transitions. Notably, the 1,5-dienoyl-CoA induced W(V) signal was never observed with dithionite or Ti(III)-citrate as reductants (5 mM each at pH 8). To elucidate the unknown redox potential of the W(IV/V) redox couple, EPR spectra were monitored at different initial benzoyl-CoA/1,5-dienoyl-CoA ratios. A clear dependence of the W(V)−OH signal on the benzoyl-CoA/1,5-dienoyl-CoA ratios and, thus, on the redox potential was observed (Figure 3). At 100% of added benzoyl-CoA (1 mM), only a minor resting state EPR signal was observed. The 1,5-dienoyl-CoA induced W(V)−OH signal gradually increased with increasing initial 1,5-dienoyl-CoA/benzoyl-CoA ratios. A plot of the W(V) signal to a Nernst curve with $E^{\circ\prime}$ = −622 mV for the benzoyl-CoA/1,5-dienoyl-CoA couple and n = 2 gave a very good fit to an apparent midpoint potential of $E^{\circ\prime}$ around −580 mV for the W(VI/V) redox couple. However, this value has to be taken rather as an estimate due to the high ratio of enzyme/CoA esters and due to the formation of 1-monoenoyl-CoA as a result of a slow disproportionation activity of Bam(BC)$_2$ (two 1,5-dienoyl-CoA → benzoyl-CoA + 1-monoenoyl-CoA).[14] Assuming that the W(V) species was diminished at pH 9 due to its reduction to W(IV) (Figure S3), the redox potentials are estimated to $E^{\circ\prime}$ = −580 mV ± 20 mV for the W(VI/V) and $E^{\circ\prime}$ = −680 mV ± 20 mV for the W(V/IV) transition. These values are the most negative ones for a tungsten- or molybdenum-enzyme; reported midpoint potentials of catalytically competent W/Mo(IV/V) transitions are generally >−500 mV (Table S1). The only exception is a spin-coupled W(V) species in GAPOR of *Pyrococcus furiosus* for which a midpoint potential of $E^{0\prime}$ = <−507 mV for the W(V/IV) transition and of $E^{0\prime}$ = −491 mV for the W(VI/V) transition has been determined at pH 7.8.[38−41]

1,5-Dienoyl-CoA-Dependent Radical Signal Cannot Be Assigned to a True Substrate or Pyranopterin-Derived Radical Species. The 1,5-dienoyl-CoA-dependent W(V)−OH intermediate was always accompanied by an isotropic EPR signal which accounted for 4−8% of the W(V) species. To test whether it can be assigned to the predicted neutral substrate radical intermediate, studies were carried out with ring-$^{13}C_6$-labeled 1,5-dienoyl-CoA. No hyperfine structure or broadening of the signal was observed (Figure S4). In a further experiment, we tested the possibility that the signal derives from a pyranopterin-based radical species as suggested by previous calculations.[25] Notably, a molybdopterin radical cation has already been experimentally verified in bacterial aldehyde dehydrogenases.[42] For this purpose, cells were grown with ^{15}N-nitrate as a terminal electron acceptor during growth of *G. metallireducens* with benzoate (nuclear spin of ^{15}N is I = 1/2). The amount of ^{15}N-nitrate added should allow for at least an 85% labeling of *G. metallireducens* cells with ^{15}N. After incubation of the resulting ^{15}N-Bam(BC)$_2$ with 1,5-dienoyl-CoA, no significant hyperfine coupling and/or broadening of the radical signal was observed (Figure S4).

Though the appearance of the radical signal strictly depended on the reduction of the enzyme with 1,5-dienoyl-CoA, its nature cannot be determined unambiguously by using isotopically labeled substrate or cofactor. The most likely scenario is that the observed signal derives from an unpaired electron that is highly delocalized over the substrate, both pyranopterin moieties of the W-*bis*-MPT and probably also over the nearby [4Fe−4S] cluster of BamB, which is substantiated by rapid freeze quench studies (see below). Notably, the [4Fe−4S] cluster was not considered in previous calculations that predicted the radical intermediates.[25] The suggested high delocalization of one-electron reduced intermediates hampers their assignment to distinct redox species but is considered the key to overcome the extremely low one-electron reduction potential of benzoyl-CoA of $E^{\circ\prime}$ = −1.9 V (vs SHE).[27]

Molecular Variants of BamB Substantiate the Role of His260 as a Proton Donor for Enzymatic Birch Reduction. The current model of enzymatic Birch reduction by class II BCRs suggests that His260 plays a crucial role in

https://doi.org/10.1021/acscatal.3c01781
ACS Catal. 2023, 13, 8631−8641

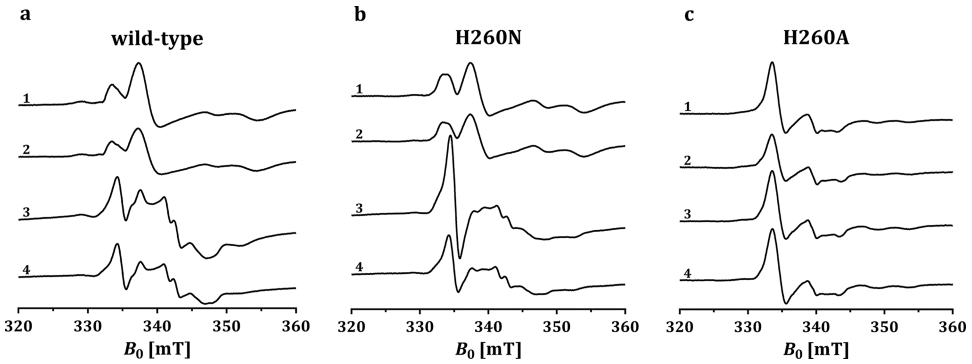

Figure 4. Study of the 77 K EPR signals of wild type Bam(BC)$_2$ and two variants. (a) Wild type, (b) His260Asn (H260N) variant, and (c) His260Ala (H260A) variant. (1) As isolated, (2) incubated with inhibitor 1-monoenoyl-CoA, (3) incubated with 1,5-dienoyl-CoA at 4 °C for ∼1 min, and (4) incubated with 1,5-dienoyl-CoA, for 5 min at room temperature. All spectra were recorded at 5 mW microwave power, 0.3 mT modulation amplitude, 100 kHz modulation frequency, and 81.92 ms conversion time. All spectra were normalized to 9.40 GHz microwave frequency for comparison.

assisting the second electron transfer to a one-electron reduced radical intermediate (Figure 1c).[25] To provide experimental evidence for this assumption and to enhance the possibility to capture EPR-detectable intermediate states, we used side-directed mutagenesis to create the two plasmids encoding the molecular variants His260Asn (pGM2087e6) and His260Ala (pGM2087e7). While wild type BamB along with BamC was homologously produced with a Strep-tag in *G. metallireducens* growing on benzoate and nitrate, the two variants His260Asn and His260Ala (again together with BamC, respectively) were cultivated with CHC as a carbon source. CHC catabolism involves the same enzymes as for benzoate degradation with the exception of the genes encoding the class II BCR complex.[30] This system allows the expression of genes encoding inactive BamB variants without a significant interference with growth. The wild type and the two variants were enriched in a soluble form under strictly anaerobic conditions via affinity chromatography (Figure S1). Activity of the BamB variants was determined by measurement of the reverse 1,5-dienoyl-CoA/methyl viologen oxidoreductase (DCO) activity.[22] While the His260Ala variant was apparently inactive (<0.01% of wild-type activity), the His260Asn variant still retained a minor activity of ≈4%.

We then compared 77 K EPR spectra of the Bam(BC)$_2$ wild type and the His260Asn and His260Ala variants in the as isolated state and after incubation with the product 1,5-dienoyl-CoA or the inhibitor 1-monoenoyl-CoA (Figure 4). The wild type and His260Asn variant showed identical EPR spectra in the as isolated state and in the presence of the inhibitor 1-monoenoyl-CoA; it is assigned to the resting W(V) signal. Upon addition of 1,5-dienoyl-CoA at 4 °C (incubation until freezing approximately 90 s after mixing), EPR spectra of both, the wild type and His260Asn, showed the typical features of the 1,5-dienoyl-CoA induced W(V) and the accompanying radical signal. However, the ratio of both was markedly altered with the relative eightfold increase of the radical vs the W(V) species. After prolonged incubation (5 min at room temperature before freezing), both signals showed a comparable W(V)/radical ratio, indicating that in both samples equilibrium was reached.

In contrast, the catalytically inactive His260Ala showed an altered resting W(V) signal, which did not change upon the addition of either the inhibitor 1-monenoyl-CoA or 1,5-dienoyl-CoA. This suggests, that the His260Ala variant most probably exhibits an altered, inactive substrate binding cavity compared to the wild type and variant His260Asn and is probably incompetent to bind a CoA-ester.

The results obtained underpin the essential role of the His260 residue in catalysis. The marked relative increase in intensity of the radical vs W(V) signal in the His260Asn variant vs wild type is in agreement with the model that His260 serves as a proton donor assisting the second electron transfer to the substrate. Thus, as a result of a hampered protonation, the one-electron reduced radical intermediate accumulates.

At first glance, it appears surprising that Asn is competent to replace His260 as a proton donor because the pK_a for direct side chain amide deprotonation is too high (≈ 16) and that of the conjugated acid (R−CONH$_3^+$ ↔ R−COH$^+$NH$_2$) is too low (≈ 0). However, Asn and Gln residues have indeed been described to be involved in proton transfer.[43,44] In QM/MM calculations, the energy profile was compared between the wild-type and the His260Asn (Figure S5). Using the program McVol,[45] space for one water molecule was found in the active site of BamB His260Asn. It occupies the free space otherwise filled by His260 and might facilitate proton transfer and stabilization of a R−COH$^+$NH$_2$ species. Though the energy barrier for 1,5-dienoyl-CoA oxidation was found higher in the His260Asn variant, it was still comparable to the WT (Figure S5). Thus, His260Asn with 1,5-dienoyl-CoA bound can feature similar cationic pyranopterin radical species as the WT enzyme. Hypothetical reaction mechanisms, in which either Glu251 or W−OH/W═O abstract the first proton of 1,5-dienoyl-CoA were ruled out since the respective energy profiles showed unrealistic or prohibitive barriers (data not shown).

W(V)−OH/Radical Intermediates Are Kinetically Competent. We further tested the kinetic competence of the observed 1,5-dienoyl-CoA induced W(V)−OH and radical species. For this purpose, millisecond RFQ and MHQ approaches were conducted to follow the time-dependent appearance of pre-steady-state intermediates. To improve the signal-to-noise ratio, these experiments were performed in D_2O. The enzyme was rapidly mixed with 1,5-dienoyl-CoA in D_2O buffer under anaerobic conditions, and the reaction was quenched at different time points in the 0.1 to 3000 millisecond range. In the following, results from RFQ (22 °C reaction temperature) and MHQ (9 °C reaction temperature) experiments were normalized to 9 °C according to the Arrhenius equation as described.[46] The rate of 1,5-dienoyl-

https://doi.org/10.1021/acscatal.3c01781
ACS Catal. 2023, 13, 8631−8641

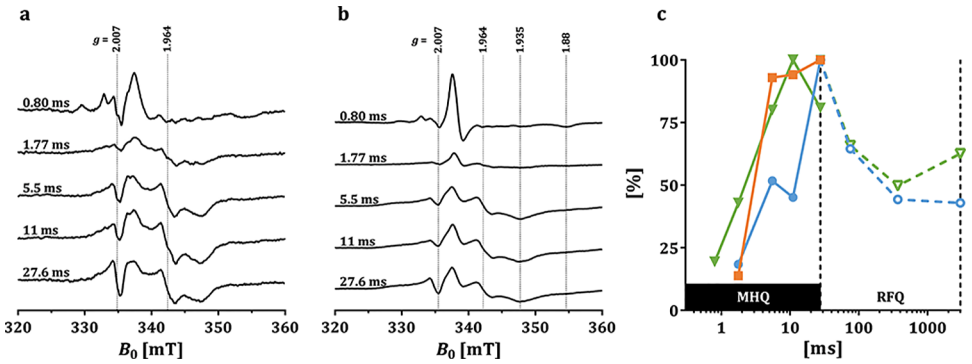

Figure 5. Pre-steady state EPR spectroscopy of Bam(BC)$_2$. (a) MHQ EPR spectra recorded at 45 K at the time points as indicated. (b) MHQ EPR spectra recorded at 15 K. (c) Time-dependent relative intensities of specific EPR signal features. Solid lines and filled symbols on the left panel represent data from MHQ EPR spectra; dotted lines and hollow symbols represent data from RFQ EPR spectra. (Inverted green triangle) MHQ EPR spectra of W(V) at g = 1.964, (solid blue circle) MHQ spectra of the isotropic radical species at g = 2.007, (orange square) MHQ spectra of the feature at 2.037 assigned to the magnetically interacting BamB [4Fe−4S]$^+$ cluster, (inverted green triangle) RFQ EPR spectra of W(V) at g = 1.964, (blue circle) MHQ spectra of the isotropic radical species at g = 2.007. All spectra were measured at 9.405 GHz microwave frequency with 5 mW power, 0.3 mT (45 K) or 0.6 mT (15 K) modulation amplitude and 100 kHz modulation frequency.

CoA aromatization by Bam(BC)$_2$ in the absence of an external electron acceptor is ≈7 s^{-1} normalized to 9 °C,[14] giving one turnover in around 140 ms. Spectra were recorded at 45 K and 15 K (MHQ) or 77 K (RFQ).

Using the MHQ setup, Bam(BC)$_2$ quenched 0.13 ms after mixing with 1,5-dienoyl-CoA showed similar features to the control sample 0.13 ms after mixing with buffer without 1,5-dienoyl-CoA (Figure S6a). Both showed the features of the resting signal observed in the as isolated state (see Figure 2a). At 0.80 ms, the resting signal was still present to a minor extent, but additional features of the 1,5-dienoyl-CoA W(V) and radical signal appeared that are observed in the D_2O buffer in the steady state (Figures 5a,c and S6b). With increasing reaction time, the resting signal fully disappeared, and both the W(V) and radical signal gradually increased and reached a maximum in the 11 ms sample. After prolonged incubation, both signals decreased again to ≈50% of the maximal value, and stayed constant after 300 ms, when the equilibrium was apparently reached. Remarkably, the rise of the W(V)/radical signal was accompanied by the broad wings that were also observed in the steady-state samples (g = 2.037 and 1.896, Figure 2b). They were assigned to the magnetically interacting [4Fe−4S]$^{+1}$ cluster near the proximal pyranopterin (Figure 5b,c). This finding supports the involvement of the BamB [4Fe−4S] cluster in the first electron transfer at the active site, which corroborates the assumed delocalization of the radical intermediate. None of the fast-relaxing EPR signals assigned to the three other [4Fe−4S]$^+$ clusters of the BamC subunits (see Figure 2b) were observed in the pre-steady state. This finding is consistent with the assumption that these clusters are not involved in catalysis but rather in electron transfer to/from the active site.

In summary, the concerted pre-steady state appearance of the W(V), radical, and [4Fe−4S]$^+$ cluster signals indicate that the proposed radical intermediate is delocalized across the entire W-*bis*-MPT and the [4Fe−4S] cluster near the proximal pyranopterin. The maximal development of the three signals after about 1/12 of one catalytic cycle demonstrates their kinetic competence.

Next, we recorded MHQ spectra of the Bam(BC)$_2$ His260Asn mutant after selected reaction times under the same conditions as the wild-type enzyme. Even after 1.77 ms, no clear W(V) signal but a small radical signal was observed reflecting that the activity is only 4% of the wild type. At 27.6 ms, both signal species were observed (not shown). In contrast to the wild type, the intensity of the radical signal increased continuously with time, even after the apparent equilibrium had been reached, whereas the W(V) signal remained constant at a lower level (Figure S7). Obviously, the spin density is differentially distributed in the His260Asn variant compared to the wild type with a shift toward the radical vs the W(V) species. This finding can be rationalized by an impaired protonation assisting the second electron transfer in the forward direction.

Unusual Reduced State Conformation of Both Pyranopterins Is Essential for the Reversibility of Catalysis. In all members of the *bis*-MPT containing dimethyl sulfoxide reductase (DMSOR) and AOR enzyme families, the proximal pyranopterin is in the reduced tetrahydro and the distal one in the oxidized dihydro form.[47] BamB is unique in binding both pyranopterins of the W-*bis*-MPT in the reduced tetrahydroform.[23] To investigate the influence of the pyranopterin oxidation state on BamB catalysis, QM/MM calculations were performed (Figures S8 and 6). For this purpose, the distal (D) and/or proximal (*P*) pyranopterins were oxidized in silico by deleting hydrogen atoms at C14 and N15, generating the 10,10a-dihydro form.[47]

While the overall reaction energy appears to be feasible in principle in direction of benzoyl-CoA reduction for all three scenarios, there are marked differences. When both pyranopterins are oxidized, the energy barrier is >4 kcal mol^{-1} higher, which should substantially slow down the reaction. When only the proximal pyranopterin is reduced, as it is the case for all other DMSOR and AOR members, the energy barrier would even be lower in comparison to the double reduced state of wild-type BamB. However, the overall reaction now becomes essentially irreversible which is in full contrast to what has been observed for BamB catalysis.[14] Previous calculations favored a mechanism in which the W atom shuttles only between the +V and +IV oxidation states. As a consequence, the second electron derives from the entire cofactor including both pyranopterin and the tungsten ion, with the resulting cationic radical being delocalized over both pyranopterins. While according to the calculations of the present work this could

https://doi.org/10.1021/acscatal.3c01781
ACS Catal. 2023, 13, 8631−8641

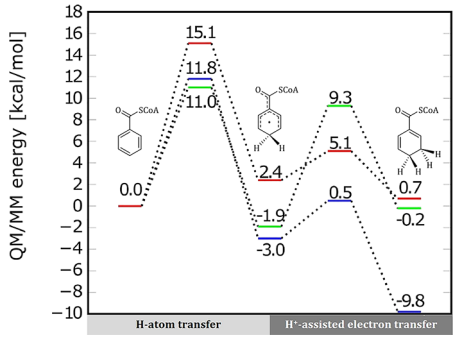

Figure 6. Dependence of the reaction energy profiles of BamB catalyzed benzoyl-CoA reduction on the redox state of the proximal (P) and distal (D) pyranopterins. Green: BamB wild type with D and P in the tetrahydro form; blue: P in tetrahydro, D in dihydro form; and red: P and D in the dihydro form.

in principle also be accomplished by one reduced pyranopterin, the resulting product bound state would be much lower in energy, thereby creating a substantial energy barrier for the initiation of a new catalytic cycle. In summary, the unusual tetrahydro state of both pyranopterins reflects the unusual low-potential one-electron transfer chemistry during enzymatic Birch reduction that is not required for other members of the DMSOR and AOR family.

CONCLUSIONS

Considering the harsh conditions of the Birch reduction of arenes to cyclic dienes, mechanistic insights into enzymatic solutions for such a process are of great importance. In this work, we provide direct EPR spectroscopic evidence for a Birch-like mechanism of enzymatic reduction of a benzenoid moiety to a conjugated cyclic diene. The identification of a catalytically competent W(V)−OH species along with a radical intermediate is in full agreement with structure- and computation-based predictions. Although the delocalization of the radical intermediate precludes detection at a defined center, a body of evidence supports that it is a true reaction intermediate during enzymatic Birch reduction: (i) The isotropic radical species appeared only in the presence of 1,5-dienoyl-CoA (reverse reaction), but never with any artificial reductant. (ii) It is kinetically competent and appeared in parallel to the W(V) species and a $[4Fe{-}4S]^{+}$ cluster. It was maximally developed after approximately 1/12 of a single turnover. (iii) It accumulates eightfold in the His260Asn mutant. In this mutant with only 4% of wild-type activity, proton-assisted second electron transfer to the radical intermediate becomes rate-limiting resulting in the observed accumulation of the latter.

In the biological solution for a Birch reduction of aromatic rings, unfavorable true single electron transfers far outside the biological redox window have to be circumvented. In class II BCRs, this is achieved in two different manners for the two individual electron transfer steps per reaction cycle. The first electron is transferred as a hydrogen atom from the W(IV)−OH_2 species yielding the W(V)−OH and radical intermediate identified in this work. This one-electron reduced intermediate is stabilized over the aromatic ring including the thioester carbonyl, the entire W-*bis*-MPT cofactor, and the [4Fe−4S] cluster in close proximity to the proximal pyranopterin. This delocalization will largely facilitate the first hydrogen atom transfer. The second electron transfer is achieved by proton-assisted electron transfer involving the catalytic His260; its substitution by an asparagine results in a 25-fold decrease of activity and an ≈8-fold increase of the radical/W(V) signal intensities. The unique presence of two pyranopterins in the reduced tetrahydro conformation in BamB appears to be crucial for maintaining the experimentally observed reversibility of the reaction and most probably for the extremely low redox potential of the W(VI/V/IV) transitions.

ASSOCIATED CONTENT

Supporting Information

The Supporting Information is available free of charge at https://pubs.acs.org/doi/10.1021/acscatal.3c01781.

Purification of enzymes, additional EPR data and computational analyses, comparison of redox potentials of tungstoenzymes, and list of plasmids used (PDF)

AUTHOR INFORMATION

Corresponding Author

Matthias Boll − *Microbiology, Faculty of Biology, Albert-Ludwigs-University Freiburg, 79104 Freiburg, Germany;* orcid.org/0000-0001-8062-8049; Email: matthias.boll@biologie.uni-freiburg.de

Authors

Carola S. Seelmann − *Microbiology, Faculty of Biology, Albert-Ludwigs-University Freiburg, 79104 Freiburg, Germany*

Simona G. Huwiler − *Microbiology, Faculty of Biology, Albert-Ludwigs-University Freiburg, 79104 Freiburg, Germany;* orcid.org/0000-0002-4876-9308

Martin Culka − *Computational Biochemistry, University of Bayreuth, 95447 Bayreuth, Germany;* orcid.org/0000-0002-3944-152X

Marc J. F. Strampraad − *Department of Biotechnology, Delft University of Technology, Delft 2629 HZ, The Netherlands*

Till Biskup − *Institute of Physical Chemistry, Albert-Ludwigs-University, 79104 Freiburg, Germany*

Stefan Weber − *Institute of Physical Chemistry, Albert-Ludwigs-University, 79104 Freiburg, Germany;* orcid.org/0000-0003-4090-7435

G. Matthias Ullmann − *Computational Biochemistry, University of Bayreuth, 95447 Bayreuth, Germany;* orcid.org/0000-0002-6350-798X

Volker Schünemann − *Department of Physics, RPTU Kaiserslautern-Landau, 67663 Kaiserslautern, Germany*

Peter-Leon Hagedoorn − *Department of Biotechnology, Delft University of Technology, Delft 2629 HZ, The Netherlands;* orcid.org/0000-0001-6342-2022

Antonio J. Pierik − *Department of Chemistry, RPTU Kaiserslautern-Landau, 67663 Kaiserslautern, Germany;* orcid.org/0000-0002-1509-6370

Complete contact information is available at: https://pubs.acs.org/10.1021/acscatal.3c01781

Author Contributions

C.S.S. purified enzymes, conducted mutagenesis experiments, prepared samples for equilibrium and RFQ and MHQ EPR experiments, carried out EPR experiments, evaluated data, and contributed to the writing of the manuscript. S.G.H. purified enzymes, prepared samples for equilibrium EPR, ran simulations, and conducted and evaluated EPR experiments.

https://doi.org/10.1021/acscatal.3c01781
ACS Catal. 2023, 13, 8631−8641

M.C. and G.M.U. carried out, evaluated QM/MM calculations, and wrote the computational part of the manuscript. T.B. and S.W. conducted and evaluated initial equilibrium EPR experiments. V.S. prepared samples for RFQ EPR experiments. M.J.F. and P.L.H. conducted and evaluated MHQ EPR experiments. A.J.P. conceived and conducted advanced equilibrium and RFQ EPR experiments, and evaluated EPR data. M.B. conceived and coordinated the project, supervised coworkers at Freiburg, wrote major parts of the manuscript, and provided project funding.

Notes

The authors declare no competing financial interest.

■ ACKNOWLEDGMENTS

We thank Jonathan Fuchs (University of Freiburg) for providing enriched class I BCR for enzymatic synthesis of 1,5-dienoyl-CoA and Lukas Knauer (RPTU Kaiserslautern-Landau) for assistance during the preparation of RFQ samples. A.J.P. acknowledges the DFG (PI610/2-2 and project ID 444947649, INST 248/320-1 FUGG) and the government of Rhineland-Palatinate for the upgrade of the EPR spectrometer. This work was supported by the Deutsche Forschungsgemeinschaft (DFG, German Research Foundation) within CRC 1381, Project ID 403222702.

■ REFERENCES

(1) Birch, A. J. Reduction by Dissolving Metals. *J. Chem. Soc.* **1942**, *430*, 430−436.
(2) Birch, A. J. The Birch Reduction in Organic Synthesis. *Pure Appl. Chem.* **1996**, *68*, 553−556.
(3) Costanzo, M. J.; Patel, M. N.; Petersen, K. A.; Vogt, P. F. Ammonia-Free Birch Reductions with Sodium Stabilized in Silica Gel, Na−SG(I). *Tetrahedron Lett.* **2009**, *50*, 5463−5466.
(4) Lei, P.; Ding, Y.; Zhang, X.; Adijiang, A.; Li, H.; Ling, Y.; An, J. A Practical and Chemoselective Ammonia-Free Birch Reduction. *Org. Lett.* **2018**, *20*, 3439−3442.
(5) Donohoe, T. J.; House, D. Ammonia Free Partial Reduction of Aromatic Compounds Using Lithium Di-Tert-Butylbiphenyl (LiDBB). *J. Org. Chem.* **2002**, *67*, 5015−5018.
(6) Burrows, J.; Kamo, S.; Koide, K. Scalable Birch Reduction with Lithium and Ethylenediamine in Tetrahydrofuran. *Science* **2021**, *374*, 741−746.
(7) Nandi, P.; Dye, J. L.; Jackson, J. E. Birch Reductions at Room Temperature with Alkali Metals in Silica Gel (Na2K-SG(I)). *J. Org. Chem.* **2009**, *74*, 5790−5792.
(8) Ishifune, M.; Yamashita, H.; Kera, Y.; Yamashita, N.; Hirata, K.; Murase, H.; Kashimura, S. Electroreduction of Aromatics Using Magnesium Electrodes in Aprotic Solvents Containing Alcoholic Proton Donors. *Electrochim. Acta* **2003**, *48*, 2405−2409.
(9) Peters, B. K.; Rodriguez, K. X.; Reisberg, S. H.; Beil, S. B.; Hickey, D. P.; Kawamata, Y.; Collins, M.; Starr, J.; Chen, L.; Udyavara, S.; Klunder, K.; Gorey, T. J.; Anderson, S. L.; Neurock, M.; Minteer, S. D.; Baran, P. S. Scalable and Safe Synthetic Organic Electroreduction Inspired by Li-Ion Battery Chemistry. *Science* **2019**, *363*, 838−845.
(10) Yasuda, M.; Pac, C.; Sakurai, H. Photochemical Reactions of Aromatic Compounds. 35.1 Photo-Birch Reduction of Arenes with Sodium Borohydride in the Presence of Dicyanobenzene. *J. Org. Chem.* **1981**, *46*, 788−792.
(11) Cole, J. P.; Chen, D. F.; Kudisch, M.; Pearson, R. M.; Lim, C. H.; Miyake, G. M. Organocatalyzed Birch Reduction Driven by Visible Light. *J. Am. Chem. Soc.* **2020**, *142*, 13573−13581.
(12) Boll, M.; Löffler, C.; Morris, B. E. L.; Kung, J. W. Anaerobic Degradation of Homocyclic Aromatic Compounds via Arylcarboxyl-Coenzyme A Esters: Organisms Strategies and Key Enzymes. *Environ. Microbiol.* **2014**, *16*, 612−627.
(13) Fuchs, G.; Boll, M.; Heider, J. Microbial Degradation of Aromatic Compounds- From One Strategy to Four. *Nat. Rev. Microbiol.* **2011**, *9*, 803−816.
(14) Kung, J. W.; Baumann, S.; Von Bergen, M.; Müller, M.; Hagedoorn, P. L.; Hagen, W. R.; Boll, M. Reversible Biological Birch Reduction at an Extremely Low Redox Potential. *J. Am. Chem. Soc.* **2010**, *132*, 9850−9856.
(15) Buckel, W. Enzymatic Reactions Involving Ketyls: From a Chemical Curiosity to a General Biochemical Mechanism. *Biochemistry* **2019**, *58*, 5221−5233.
(16) Unciuleac, M.; Boll, M. Mechanism of ATP-Driven Electron Transfer Catalyzed by the Benzene Ring-Reducing Enzyme Benzoyl-CoA Reductase. *Proc. Natl. Acad. Sci. U. S. A.* **2001**, *98*, 13619−13624.
(17) Tiedt, O.; Fuchs, J.; Eisenreich, W.; Boll, M. A Catalytically Versatile Benzoyl-CoA Reductase, Key Enzyme in the Degradation of Methyl- and Halobenzoates in Denitrifying Bacteria. *J. Biol. Chem.* **2018**, *293*, 10264−10274.
(18) Huwiler, S. G.; Löffler, C.; Anselmann, S. E. L.; Stärk, H.-J.; von Bergen, M.; Flechsler, J.; Rachel, R.; Boll, M. One-Megadalton Metalloenzyme Complex in *Geobacter metallireducens* Involved in Benzene Ring Reduction beyond the Biological Redox Window. *Proc. Natl. Acad. Sci. U. S. A.* **2019**, *116*, 2259−2264.
(19) Appel, L.; Willistein, M.; Dahl, C.; Ermler, U.; Boll, M. Functional Diversity of Prokaryotic HdrA(BC) Modules: Role in Flavin-Based Electron Bifurcation Processes and Beyond. *Biochim. Biophys. Acta, Bioenerg.* **2021**, *1862*, No. 148379.
(20) Buckel, W.; Thauer, R. K. Flavin-Based Electron Bifurcation, A New Mechanism of Biological Energy Coupling. *Chem. Rev.* **2018**, *118*, 3862−3886.
(21) Seelmann, C. S.; Willistein, M.; Heider, J.; Boll, M. Tungstoenzymes: Occurrence, Catalytic Diversity and Cofactor Synthesis. *Inorganics* **2020**, *8*, 44.
(22) Kung, J. W.; Löffler, C.; Dorner, K.; Heintz, D.; Gallien, S.; Van Dorsselaer, A.; Friedrich, T.; Boll, M. Identification and Characterization of the Tungsten-Containing Class of Benzoyl-Coenzyme A Reductases. *Proc. Natl. Acad. Sci. U. S. A.* **2009**, *106*, 17687−17692.
(23) Weinert, T.; Huwiler, S. G.; Kung, J. W.; Weidenweber, S.; Hellwig, P.; Stärk, H. J.; Biskup, T.; Weber, S.; Cotelesage, J. J. H.; George, G. N.; Ermler, U.; Boll, M. Structural Basis of Enzymatic Benzene Ring Reduction. *Nat. Chem. Biol.* **2015**, *11*, 586−591.
(24) Buckel, W.; Kung, J. W.; Boll, M. The Benzoyl-Coenzyme A Reductase and 2-Hydroxyacyl-Coenzyme A Dehydratase Radical Enzyme Family. *ChemBioChem* **2014**, *15*, 2188−2194.
(25) Culka, M.; Huwiler, S. G.; Boll, M.; Ullmann, G. M. Breaking Benzene Aromaticity - Computational Insights into the Mechanism of the Tungsten-Containing Benzoyl-CoA Reductase. *J. Am. Chem. Soc.* **2017**, *139*, 14488−14500.
(26) Willistein, M.; Haas, J.; Fuchs, J.; Estelmann, S.; Ferlaino, S.; Müller, M.; Lüdeke, S.; Boll, M. Enantioselective Enzymatic Naphthoyl Ring Reduction. *Chem. − Eur. J.* **2018**, *24*, 12505−12508.
(27) Boll, M.; Laempe, D.; Eisenreich, W.; Bacher, A.; Mittelberger, T.; Heinze, J.; Fuchs, G. Nonaromatic Products from Anoxic Conversion of Benzoyl-CoA with Benzoyl-CoA Reductase and Cyclohexa-1,5-Diene-1-Carbonyl-CoA Hydratase. *J. Biol. Chem.* **2000**, *275*, 21889−21895.
(28) Oberender, J.; Kung, J. W.; Seifert, J.; von Bergen, M.; Boll, M. Identification and Characterization of a Succinyl-Coenzyme A (CoA): Benzoate CoA Transferase in *Geobacter metallireducens*. *J. Bacteriol.* **2012**, *194*, 2501−2508.
(29) Lovley, D. R.; Phillips, E. J. P. Novel Mode of Microbial Energy Metabolism: Organic Carbon Oxidation Coupled to Dissimilatory Reduction of Iron or Manganese. *Appl. Environ. Microbiol.* **1988**, *54*, 1472−1480.
(30) Kung, J. W.; Meier, A. K.; Mergelsberg, M.; Boll, M. Enzymes Involved in a Novel Anaerobic Cyclohexane Carboxylic Acid Degradation Pathway. *J. Bacteriol.* **2014**, *196*, 3667−3674.
(31) Laemmli, U. K. Cleavage of Structural Proteins during the Assembly of the Head of Bacteriophage T4. *Nature* **1970**, *227*, 680−685.

https://doi.org/10.1021/acscatal.3c01781
ACS Catal. 2023, 13, 8631−8641

(32) Bradford, M. M. A Rapid and Sensitive Method for the Quantitation of Microgram Quantities of Protein Utilizing the Principle of Protein-Dye Binding. *Anal. Biochem.* **1976**, *72*, 248−254.
(33) Stesmans, A.; van Gorp, G. Improved Measurement of the g Factor of Conduction Electrons in Li Particles Embedded in LiF:Li. *Phys. Lett. A* **1989**, *139*, 95−98.
(34) Hagen, W. R. *Biomolecular EPR Spectroscopy*; CRC Press, Taylor & Francis Group: Boca Raton, London, New York, 2009; pp 53−57.
(35) Glasoe, P. K.; Long, F. A. Use of Glass Electrodes to Measure Acidities in Deuterium Oxide. *J. Phys. Chem.* **1960**, *64*, 188−190.
(36) Stoll, S.; Schweiger, A. EasySpin, a Comprehensive Software Package for Spectral Simulation and Analysis in EPR. *J. Magn. Reson.* **2006**, *178*, 42−55.
(37) Cherepanov, A. V.; De Vries, S. Microsecond Freeze-Hyperquenching: Development of a New Ultrafast Micro-Mixing and Sampling Technology and Application to Enzyme Catalysis. *Biochim. Biophys. Acta, Bioenerg.* **2004**, *1656*, 1−31.
(38) Koehler, B. P.; Mukund, S.; Conover, R. C.; Dhawan, I. K.; Roy, R.; Adams, M. W. W.; Johnson, M. K. Spectroscopic Characterization of the Tungsten and Iron Centers in Aldehyde Ferredoxin Oxidoreductases from Two Hyperthermophilic Archaea. *J. Am. Chem. Soc.* **1996**, *118*, 12391−12405.
(39) Boll, M.; Fuchs, G.; Meier, C.; Trautwein, A.; El Kasmi, A.; Ragsdale, S. W.; Buchanan, G.; Lowe, D. J. Redox Centers of 4-Hydroxybenzoyl-CoA Reductase, a Member of the Xanthine Oxidase Family of Molybdenum-Containing Enzymes. *J. Biol. Chem.* **2001**, *276*, 47853−47862.
(40) Johnson, M. K.; Rees, D. C.; Adams, M. W. W. Tungstoenzymes. *Chem. Rev.* **1996**, *96*, 2817−2840.
(41) Hagedoorn, P. L.; Freije, J. R.; Hagen, W. R. *Pyrococcus furiosus* Glyceraldehyde 3-Phosphate Oxidoreductase Has Comparable W(6+/5+) and W(5+/4+) Reduction Potentials and Unusual [4Fe-4S] EPR Properties. *FEBS Lett.* **1999**, *462*, 66−70.
(42) Luykx, D. M. A. M.; Duine, J. A.; De Vries, S. Molybdopterin Radical in Bacterial Aldehyde Dehydrogenases. *Biochemistry* **1998**, *37*, 11366−11375.
(43) Malwal, S. R.; Gao, J.; Hu, X.; Yang, Y.; Liu, W.; Huang, J.-W.; Ko, T.-P.; Li, L.; Chen, C.-C.; O'Dowd, B.; Khade, R. L.; Zhang, Y.; Zhang, Y.; Oldfield, E.; Guo, R.-T. Catalytic Role of Conserved Asparagine, Glutamine, Serine, and Tyrosine Residues in Isoprenoid Biosynthesis Enzymes. *ACS Catal.* **2018**, *8*, 4299−4312.
(44) Akihiko, N.; Takuya, I.; Katsuhiro, K.; Taro, Y.; Shinya, F.; Ichiro, T.; Satoshi, K.; Kazunori, O.; Hiroaki, T.; Koji, I.; Yoshiki, H.; Nobuo, N.; Masahiro, S.; Kiyohiko, I. "Newton's Cradle" Proton Relay with Amide−Imidic Acid Tautomerization in Inverting Cellulase Visualized by Neutron Crystallography. *Sci. Adv.* **2015**, *1*, No. e1500263.
(45) Till, M. S.; Ullmann, G. M. McVol - A Program for Calculating Protein Volumes and Identifying Cavities by a Monte Carlo Algorithm. *J. Mol. Model.* **2010**, *16*, 419−429.
(46) Srour, B.; Strampraad, M. J. F.; Hagen, W. R.; Hagedoorn, P. L. Refolding Kinetics of Cytochrome c Studied with Microsecond Timescale Continuous-Flow UV-Vis Spectroscopy and Rapid Freeze-Quench EPR. *J. Inorg. Biochem.* **2018**, *184*, 42−49.
(47) Rothery, R. A.; Stein, B.; Solomonson, M.; Kirk, M. L.; Weiner, J. H. Pyranopterin Conformation Defines the Function of Molybdenum and Tungsten Enzymes. *Proc. Natl. Acad. Sci. U. S. A.* **2012**, *109*, 14773−14778.

https://doi.org/10.1021/acscatal.3c01781
ACS Catal. 2023, 13, 8631−8641